International Journal of Heat and Mass Transfer 60 (2013) 134–142

Contents lists available at SciVerse ScienceDirect

International Journal of Heat and Mass Transfer

journal homepage: www.elsevier.com/locate/ijhmt

Measurement of thermal conductivity and heat pipe effect in hydrophilic and hydrophobic carbon papers

Yun Wang *, Mehernosh Gundevia

Renewable Energy Resources Lab (RERL), Department of Mechanical and Aerospace Engineering, The University of California, Irvine, CA 92697-3975, USA

ARTICLE INFO

Article history:
Received 16 July 2012
Received in revised form 4 December 2012
Accepted 4 December 2012

Keywords:
Heat conductance
Experiment
Heat pipe effect
Hydrophilic
Hydrophobic
Carbon paper

ABSTRACT

In this paper, we present an experimental study on measurement of the thermal conductivity and heat pipe effect in both hydrophilic and hydrophobic (Toray TGP-H60) carbon papers (around 200 μm thickness) with/out liquid water. An experimental setup is developed for measuring thermal conductance at different liquid water contents and temperatures without dissembling the testing device for water addition. Theoretical analysis is also performed to evaluate the apparent conductance of heat pipe effect. We found that liquid water presence inside these materials increases the overall thermal conductivity. At high temperature around 80 °C, the heat pipe effect is evident for the hydrophilic paper; while for the hydrophobic one, the heat pipe effect is found to be smaller. The distinction is likely due to the different patterns of the capillary liquid flow in the two media. For the hydrophobic paper, liquid water flows back to the evaporation side when the breakthrough pressure is reached and flow is through preferred routes of small flow resistance. As a result, heat pipe effect is active only in part of the medium, therefore smaller than that in the hydrophilic one. The results are important for understanding the heat transfer phenomena occurring in porous media and effects of material surface property.

1. Introduction

Carbon papers are porous materials that are widely applied in a variety of engineering applications, such as batteries, heat transfer devices, fuel cells, multi-stage filters, high-temperature thermal insulators, and friction/wear applications. Carbon papers are nonwoven fibrous media, based on carbon fibers, and are commercially available. Carbon fibers possess excellent properties of stiffness, strength, conductivity, and light weight, and can be made from polyacrylonitrile (PAN), heavy fractions of oils or coals, cellulose, or others. In fabrication, the raw carbon fibers are carbonized at high temperature in inert environment to reduce other elements (such as nitrogen, oxygen, and hydrogen), yielding fibers with high carbon content and strong mechanical strength. In the papermaking process, the chopped carbon fibers are dispersed in water with binders, such as polyvinyl alcohol, to produce carbon paper roll. Binder content in carbon papers usually ranges from 5% to 15% by weight. The paper's porosity can be 80% or higher, e.g. Toray carbon papers. This type of carbon papers has a mean pore size of about 20 μm. Their pore network provides passages for fluid flow or species transport, while the solid matrix enables electric current conductance or heat transfer [1,2].

Carbon paper's surface property plays an important role in two-phase flow occurring inside the medium. This property can be modified through adding Polytetrafluoroethylene (PTFE), nanostructures, or other chemical agents. Applying PTFE loading is widely adopted in PEM fuel cell development. In this method, carbon papers are dipped into aqueous PTFE suspensions or by spraying. The wet papers are then placed in an oven for drying to remove the residual solvent. High temperature above 300 °C will sinter PTFE and fix it to the fiber surface. Higher PTFE content yields a more hydrophobic property. Adding PTFE, however, reduces the media's porosity and possibly the mean pore size.

Thermal conductivity is an important property of carbon papers, particularly in thermal and power applications. Though carbon fibers are highly conductive, the effective conductivity can be low when the porosity is high. The effective conductivity is also dependent on compression, PTFE loading, solid matrix's tortuosity, and the fluid materials in the void space. Various experimental methods have been employed to measure thermal conductivity [3], and can be extended to carbon papers. Khandelwal and Mench [4] measured carbon papers and Nafion membranes for PEM fuel cell. They reported a thermal conductivity of 0.22 ± 0.04 W/m °C for Sigracet® 20 wt.% PTFE carbon paper and 1.80 ± 0.27 W/m °C for Toray papers. Zamel et al. [5] measured the through-plane thermal conductivity of dry Toray papers in a range of 50–120 °C. They reported about 0.8–1.8 W/m °C conductivity at high deformation and 0.2–0.4 W/m °C at low deformation. Burheim et al. [6]

* Corresponding author. Tel.: +1 949 824 6004; fax: +1 949 824 8585.
E-mail address: yunw@uci.edu (Y. Wang).

0017-9310/$ - see front matter © 2012 Elsevier Ltd. All rights reserved.
http://dx.doi.org/10.1016/j.ijheatmasstransfer.2012.12.016

Nomenclature

C	concentration (mol/m^3)
D	diffusivity (m^2/s)
h	the latent heat (J/kg)
k	thermal conductivity (W/m °C)
K	permeability (m^2)
M	molecular weight (kg/mol)
p	pressure (pa)
S	saturation
u	velocity (m/s)
Greek symbols	
σ	surface tension (N/m)
ε	porosity
θ	contact angle (deg)
μ	viscosity (kg/m-s)
ρ	density (kg/m^3)
λ	mobility
τ	tortuosity
Subscript or superscript	
c	capillary
eff	effective
fg	phase change
g	gas
hp	heat pipe
l	liquid
sat	saturation
w	water
o	reference point

measured SolviCore porous media at various compaction pressures. For dry media under 4.6, 9.3 and 13.9 bar, the measured conductivity was 0.27, 0.36 and 0.40 W/m °C, respectively. They reported an increase of around 0.17 W/m °C in thermal conductivity when about 25% liquid saturation is present inside the media. Burheim et al. [7] reported the through-plane thermal conductivities of the several widely used carbon porous transport layers (PTLs). They found that the thermal conductivity of dry PTLs decreases with increasing PTFE content and increases with residual water.

The heat pipe effect will be promoted in carbon papers when there exists two-phase flow under a nonisothermal condition. The effect results from the transport and phase change of the working fluid flow, e.g. the vapor-phase diffusion, capillary liquid flow, condensation, and evaporation: at the evaporation side, the liquid work fluid evaporates, absorbing heat. The resulting vapor transports towards the condensation side, where the vapor condenses to liquid, releasing heat. The condensed work fluid then returns back to the evaporation side, restarting the cycle. In this process, heat is transported from the evaporation to the condensation sides. Wang and Wang [8,9] evaluated vapor-phase diffusion and heat pipe conductance, indicating that the former is a significant mechanism in the water management of PEM fuel cell and the latter contributes about 0.3–0.5 W/m °C conductivity at 80 °C. Though the carbon paper's conductivity has been measured by several experiments, little has been done experimentally to investigate the heat pipe effect and the role of liquid in the media. In this study, experiment was designed for precise control of liquid injection into a sealed sample, and measurement of heat pipe effect. By comparing the results of dry and wet carbon papers, the added thermal conductance contributed by liquid water presence, including heat pipe effect, was obtained.

2. Heat transfer and heat pipe effect in carbon papers

In carbon papers, the carbon fibers are randomly aligned in the lateral direction. In the presence of static air or hydrogen gas in the void space, a major portion of heat flow is through the solid matrix of fibers because of its high conductivity. The solid matrix's structure therefore plays an important role in heat transfer through the carbon papers.

2.1. Carbon paper microstructure

Carbon papers consist of randomly aligned carbon fibers bound by carbonized thermoset resin, see Fig. 1(a). The fiber diameter is usually around 5–10 μm. The paper's fiber structures can be reconstructed through imaging or stochastic modeling. The former uses imaging techniques, such as the X-ray Tomograph or magnetic resonance. The material is repeatedly sectioned and imaged. The images are used in software to reconstruct the detailed material's 3-D structure. The latter method is based on the knowledge of the material's structure and stochastic theory. It is cost effective and fast, and its resolution is usually limited by the reconstruction mesh. Fig. 1(b) displays the reconstructed solid matrix of a carbon paper [10], showing a highly tortuous solid matrix due to the lateral alignment of its carbon fibers. Direct simulation results revealed that the through-plane heat conduction occurs via a route combining the lateral path along fibers and through-plane one at the contact points, see Fig. 2(a), resulting in a value of about 13 for the tortuosity of the solid matrix [10], and a complex distribution of temperature, see Fig. 3. The effective conductivity can be evaluated by accounting for the volume fraction of individual phase:

$$k^{eff} = k^s(1-\varepsilon)^{\tau_s} + k^f\varepsilon^{\tau_f} \tag{1}$$

where τ is tortuosity. In the occasion that the fibrous matrix is much more conductive than the fluid in the void, the effective conductivity can be approximated by only accounting for the solid content:

$$k^{eff} = k^s(1-\varepsilon)^{\tau_s} \tag{2}$$

Adding PTFE changes the carbon paper's surface properties, and it also alters the medium's porosity, and possibly its thermal conductivity. Fig. 1(c) and (d) display the carbon papers with 0 and 30 wt.% PTFE loadings, respectively.

2.2. Vapor-phase diffusion and heat pipe effect

The pore size of commercial carbon papers such as Toray papers usually ranges from 10 to 100 μm with the mean size of about 20 μm [2]. Due to the small dimension, phase equilibrium generally holds true between vapor and liquid phases in local pores. Under an isothermal condition, this equilibrium ensures a uniform vapor partial pressure throughout the medium. In a non-isothermal environment, i.e. temperature varies spatially, local vapor-partial pressure differs spatially, leading to vapor-phase diffusion. Using a 1-D case as example, the presence of a temperature gradient will cause the following vapor-phase diffusive flux [8]:

$$-D_g^{w,eff}\frac{dC^w}{dx} = -D_g^{w,eff}\frac{dC_{sat}(T)}{dx} = -D_g^{w,eff}\frac{dC_{sat}}{dT}\frac{dT}{dx} \tag{3}$$

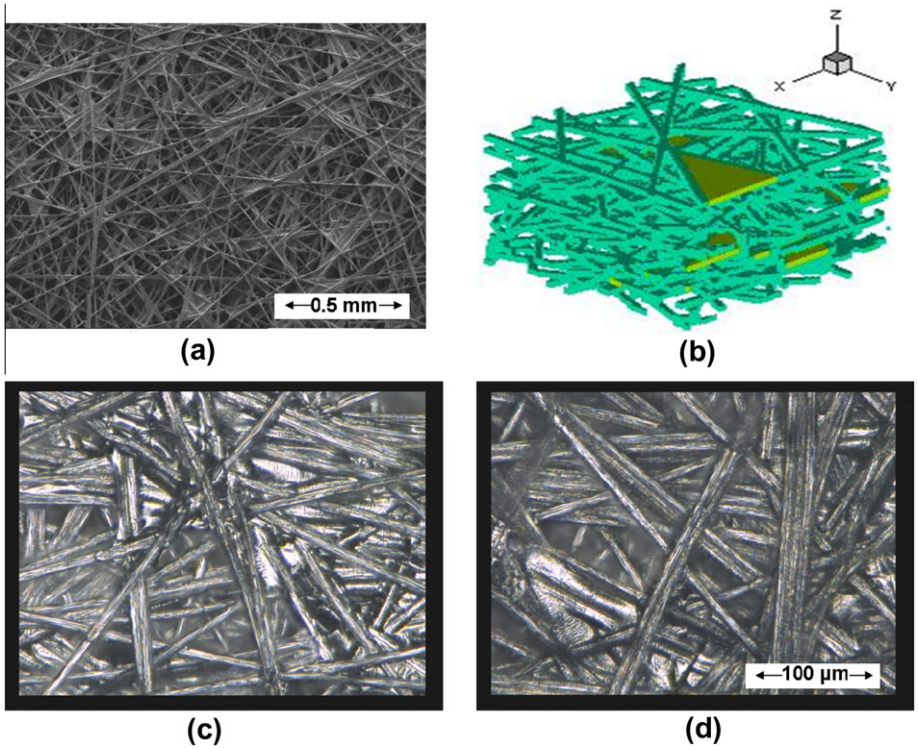

Fig. 1. (a) The surface of a carbon paper; (b) the solid matrix of a reconstructed carbon paper [10]; (c) hydrophilic carbon paper (0 wt.% PTFE loading); (d) hydrophobic carbon paper (30 wt.% PTFE loading). (c and d) are from Ref. [19].

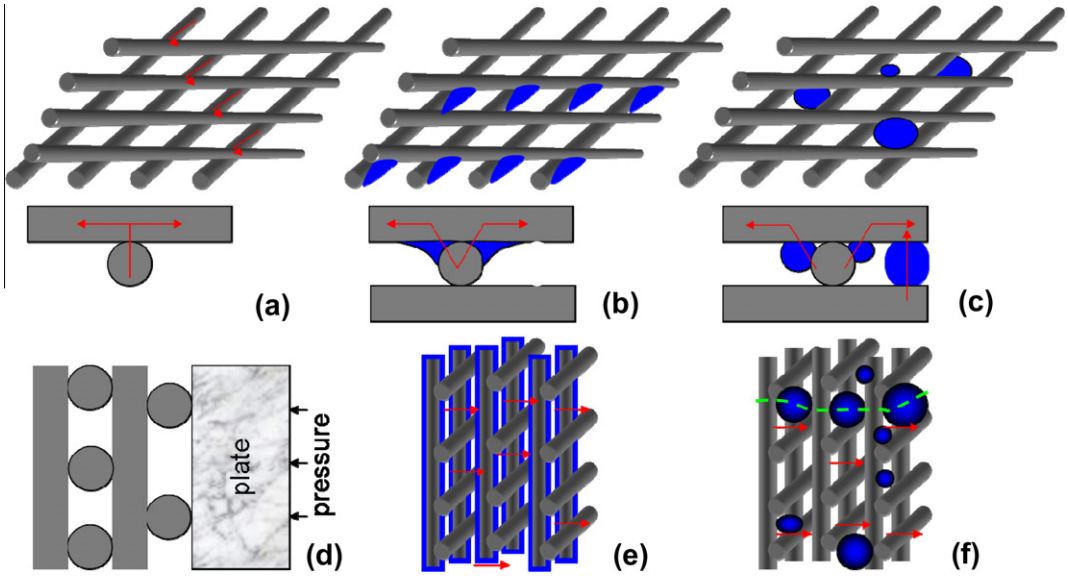

Fig. 2. Schematics of heat transfer in a dry carbon paper (a), hydrophilic carbon paper (b), and hydrophobic carbon paper (c); the contacts between the sample and plate and among fibers (d), heat flow by heat pipe effects in hydrophilic carbon paper (e) and hydrophobic carbon paper (f). The carbon fibers are intently drawn in a structural fashion for illustration purposes.

where $C_{sat}(T)$ represents the saturated water concentration, and its profile is displayed in Fig. 4 as a function of temperature. The diffusion coefficient is dependent on temperature and pressure:

$$D_g^w = D_{g,o}^w \left(\frac{T}{353}\right)^{3/2} \left(\frac{1}{P}\right) \tag{4}$$

The vapor phase contains the latent heat of evaporation, and therefore its diffusion delivers heat. This is realized by water evaporation at hotter sites, vapor diffusion through the interstitial spaces, and subsequent condensation at cooler sites. This mode of heat transfer is conventionally referred to as the heat pipe effect. In another word, the heat pipe effect here is driven by the concentration difference of water vapor imposed by a temperature difference. It involves a coupling phenomenon between transport of heat and mass. Assuming the vapor diffusion is the limiting factor in heat pipe effect, the delivered heat flux can be estimated as follow:

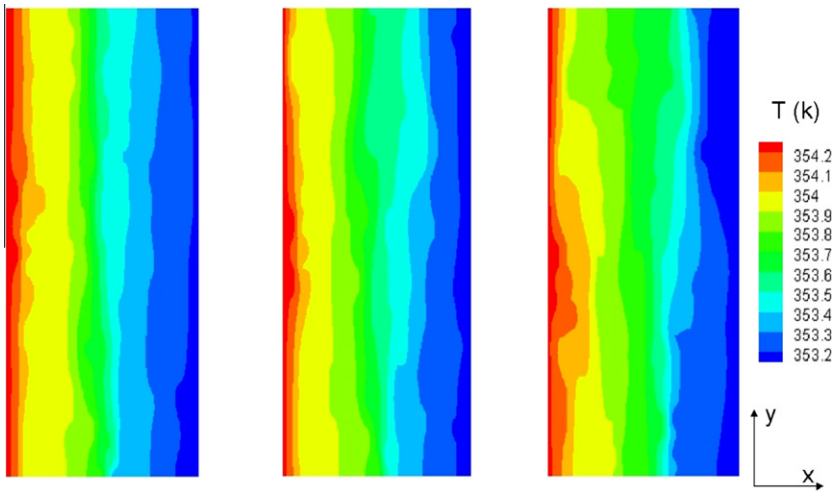

Fig. 3. Temperature distributions in three cross sections of a carbon paper, predicted by the direct simulation of heat transfer in PEM fuel cell [10]. The right side is set at 353.15 K and a heat flux due to the waste heat production by PEM fuel cell is added to the left side.

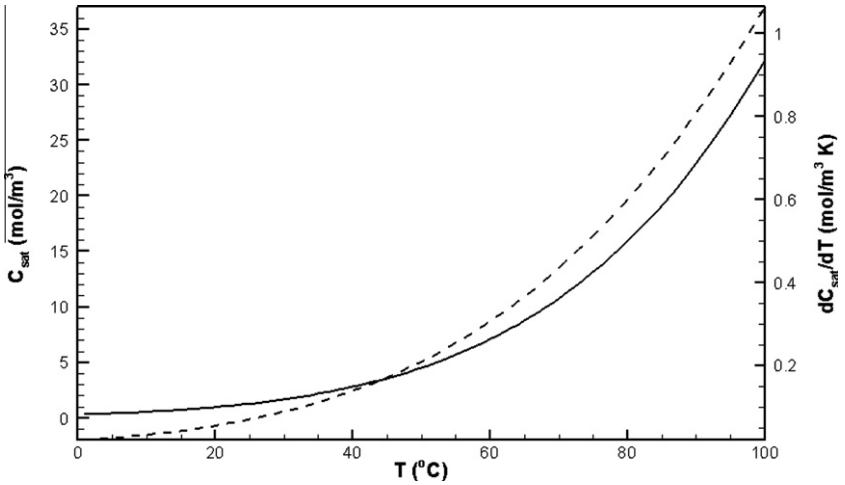

Fig. 4. The water vapor saturation concentration (the solid line) and its derivative (the dash line) as a function of temperature.

$$h_{fg}\dot{m}_{fg} = h_{fg}M_w D_g^{w,eff}(T,P)\frac{dC_{sat}(T)}{dT}\frac{dT}{dx} = k_{hp}(T,P)\frac{dT}{dx} \quad (5)$$

The above derivation indicates the heat pipe effect can be described using an apparent thermal conductivity k_{hp}. This conductivity is a function of temperature, pressure, and pore structure. Fig. 4 displays the saturation vapor concentration and its derivative, showing both rapidly increase with temperature. Fig. 5 displays the apparent conductance k_{hp} at different temperatures, calculated from Eq. (5), showing a similar trend of k_{hp} with temperature: the heat pipe effect is weak (<0.05 W/m °C) at <20 °C, and increases to 0.7 W/m °C at 80 °C for the water–air system and porosity of 0.8. Because water vapor in hydrogen gas has a higher diffusivity, the heat pipe effect is stronger, about 1 W/m °C versus 0.4 W/m °C for the water–air system at 80 °C. Because the vapor-phase diffusion occurs in the void space, the heat-pipe heat transfer is parallel to that in the solid matrix. Thus, the apparent heat conductance can be directly added to local intrinsic thermal conductivity.

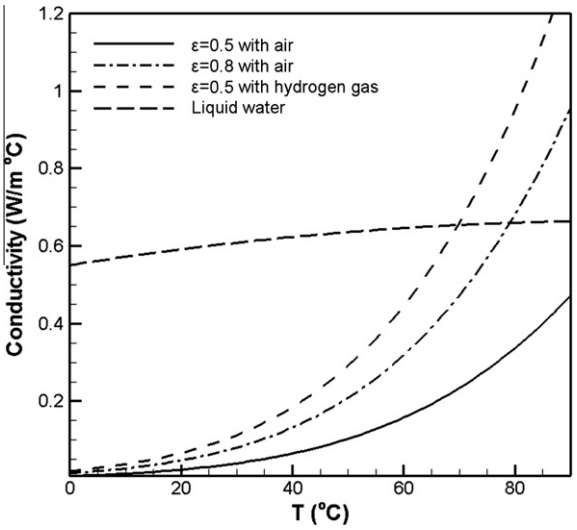

Fig. 5. Heat pipe conductance k_{hp} and bulk liquid water conductivity as a function of temperature.

2.3. Capillary flow

In addition to vapor-phase diffusion, the heat-pipe conductance is also limited by the capillary liquid flow and phase-change rates.

Table 1
List of parameters.

Quantity	Value
The compression ratio for the hydrophilic carbon paper (0 wt.% PTFE loading)	15 ± 3%
The compression ratio for the hydrophobic carbon paper (30 wt.% PTFE loading)	18 ± 3%
Sample porosity before/after compression (hydrophilic carbon paper)	0.8/0.76
Sample porosity before/after compression (hydrophobic carbon paper)	0.72/0.66
Sample area	2 × 2 cm
Pressures, P	1.0 atm
The diffusion coefficient $D^w_{g,o}$ of water vapor in air at 353 K and 1 atm [18]	3.89×10^{-5} m^2/s
The diffusion coefficient $D^w_{g,o}$ of water vapor in hydrogen gas at 353 K and 1 atm [18]	1.10×10^{-4} m^2/s
Permeability of carbon papers [1]	10^{-12} m^2
The surface tension of water in the air at 80 °C, σ [1]	0.0625 N/m
The measured contact angles θ_c for the hydrophilic and hydrophobic carbon papers	66/128°
The latent heat of water liquid–gas phase change, h_{fg} [1]	2.26×10^6 J/kg

The phase-change rate is determined by the local mass-transfer coefficient, effective surface area, and others. In carbon papers, e.g. Toray papers with their mean pore size around 20 μm, the interfacial area between the liquid and vapor phases is large, resulting in rapid phase change. The capillary flow, however, can be slow, and become a limiting factor in the heat pipe performance. The capillary flow flux $\vec{j}^{(l)}$, driven by the capillary pressure P_c and gravitational force, can be expressed as [11]:

$$\vec{j}^{(l)} = \frac{\lambda^{(l)}\lambda^{(g)}}{\nu} K[\nabla P_c + (\rho^{(l)} - \rho^{(g)})\vec{g}] \quad \text{where} \quad P^{(g)} - P^{(l)} = P_c = \sigma\cos(\theta_c)\left(\frac{\varepsilon}{K}\right)^{1/2} J(s) \tag{6}$$

where σ is the surface tension, θ_c the contact angle, ν the kinematic viscosity, λ the phase mobility, K the permeability, and s the liquid saturation. The Leverett-J function $J(s)$ for hydrophilic media is given by:

$$J(s) = 1.417(1-s) - 2.120(1-s)^2 + 1.263(1-s)^3 \qquad \text{for } \theta_c < 90^\circ \tag{7}$$

It should be pointed out that the above Leverett function was originally developed to describe liquid–water transport in soils; as such, it is not directly applicable to the liquid water transport in carbon papers due to their unique fibrous characteristics. Kumbur et al. [12] showed the above Leveret function exhibits significant deviation from their experimental data, and developed new Leveret functions that better fit with the data. Gostick et al. [13] proposed a new correlation for the capillary pressure for fibrous porous media as well. In addition, the capillary flow in hydrophobic media can be different. Though continuum models were proposed for hydrophobic carbon papers, the actual two-phase flow is usually highly dynamic, and difficult to predict. Several studies visualized liquid water flow through hydrophobic media, showing liquid flows via preferred routes when the breakthrough pressure is reached. Before reaching the breakthrough pressure, liquid water is stuck inside the medium and remains static. The stuck water is similar to the irreducible residual liquid that is bound inside the pores by surface tension force and hence cannot be removed by drainage but only by evaporation.

3. Experimental

To measure the thermal conductivity of carbon papers and heat pipe effect, the experiment was designed as shown schematically in Fig. 6. The experimental setup consists of housing for the carbon paper sample, a gasket for seal, a cooling plate for heat removal, a hot plate, and an insulation enclosure to prevent heat loss during measurement. The cooling plate is made of aluminum with grooved mini serpentine channels for cooling flow fed by a self-designed high-precision flow injector. The cooling flow rate is injected under control with uncertainty as low as 0.01 mL/min. By measuring the inlet and outlet flows' temperatures, the heat removal rate, i.e., the heat flow across the sample and gasket, can be obtained. A micro channel was machined in the housing plate to enable liquid injection by a high-precision syringe with an accuracy of 0.002 mL (equivalent to ~5% saturation in samples). Four thermocouples were used to measure the temperatures of the two sample surfaces with an uncertainty of 0.05 °C. The uncertainty of conductivity measurement is about 0.03 W/m °C [11]. In testing, we use Toray papers (TGP-H60) with 0 and 30 wt.% PTFE, respectively. Fig. 1(c) and (d) show these two media; and Fig. 7 displays the droplet shapes at the medium surfaces, through which the contact angles were measured to be about 66° and 128°, respectively. In the experiment, the two media were compressed by 15 ± 3% and 18 ± 3% in thickness, respectively. We choose to use the compression ratio instead of the compaction pressure because a PTFE gasket is used to seal the sample. The portion of the compaction pressure acting on the sample is therefore unknown and difficult to determine. Several studies investigated the relative compression ratio, compaction pressure, and effective thermal conductivity of GDL materials [1,5,7,14], which may provide a way to estimate the compaction pressure over the sample. Readers who are interested in these subjects are referred to these articles. The entire device is insulated by insulation foam with 1 cm thickness. The sample through-plane conductivity is calculated via Fourier's law using the measurements of the heat flow through the sample, the surface temperatures, and the sample area and thickness. Several materials with known thermal conductivity, such as printing papers and PTFE sheets, were tested using the device, showing good accuracy. (Table 1) lists several major experimental parameters.

In the experiment, the contact resistance between the sample and plates and among fibers can be large upon insufficient compression due to the use of gasket. Fig. 2(d) shows the fibers and their contact with a plate: the contact resistance arises not only between the carbon paper and plate which is the conventional meaning of contact resistance, but also among the constituent fibers. A high compression will yield a better contact or a large contact area both between the sample and plate, and among papers. As explained before, the fiber-to-fiber contact area can be a limiting factor for the through-plane conductivity. We assume the contact resistance distributes uniformly throughout the sample. In other words, the sample's intrinsic conductivity is dependent on the pressure imposed over its surface. This is similar to unsolidified packed beds, whose conductivity increases with compression due to the enhanced contact among particles. Using spherical particles as example, a compressed state exhibits higher overall thermal conductivity than a loosely packed state, because the contact among particles is tighter in the former case. If this holds true for the carbon paper, the presented contact resistance then has no effect on the measurement of heat pipe effect and liquid water influence because the contact resistance is cancelled out when comparing the dry sample's measurement with the wet one, to be discussed later in this section. To change the sample temperature, external heated flow is fed in the hot flow plate. It took up to one hour for the device to reach steady state. Measurement was taken when no temperature change was observed in 10 min.

In the experimental procedure, measurement was conducted first on a dry sample. Neglecting the air's contribution to conductance, the overall effective conductivity can be expressed by:

$$k^{eff}_{dry} = k^s(1-\varepsilon)^{\tau_s} \tag{8}$$

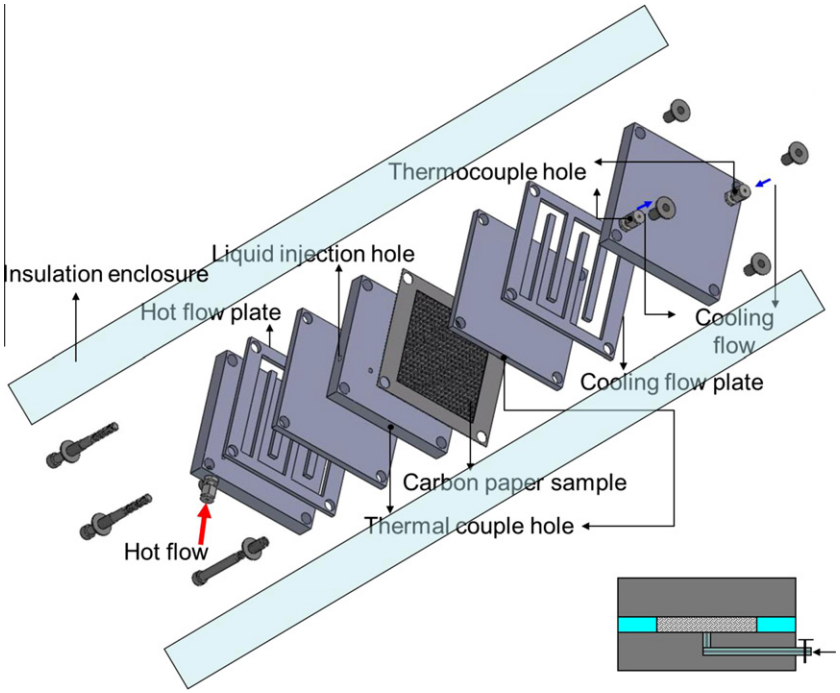

Fig. 6. Schematic of the experimental set up for thermal conductivity measurement. The right corner shows the liquid water injection to the sample.

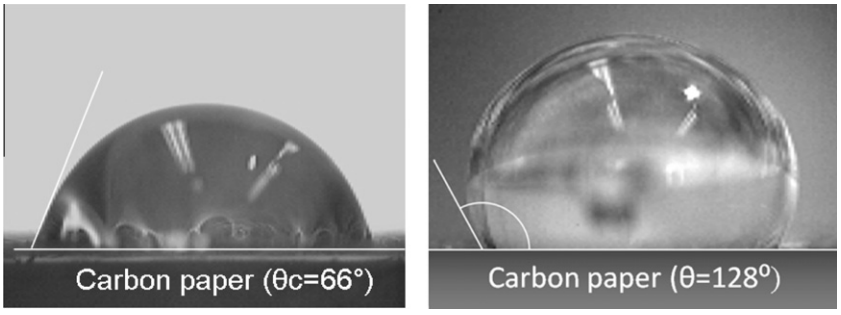

Fig. 7. Liquid water droplets at the surfaces of the hydrophilic and hydrophobic carbon papers [19].

After the dry sample is measured, a controlled amount of liquid water was then injected into the sample without dissembling the device. The wet sample conductivity can then be expressed by:

$$k_{wet}^{eff} = k^{s}(1-\varepsilon)^{\tau_s} + \varepsilon^{\tau_l} k^{l} + k_{hp} \tag{9}$$

The above takes into account the added thermal conductance due to liquid water presence $\varepsilon^{\tau_l} k^{l}$ and heat pipe effect k_{hp}. Added liquid can influence the overall thermal conductivity in several ways, such as liquid location (e.g. near the fibers joints) and shape (e.g. contact angle). Burheim et al. [7] presented a discussion on the contribution of liquid water. Those factors can be lumped in the parameter of tortuosity, which characterizes the transport path. Comparing the two measurements yields:

$$k_{wet}^{eff} - k_{dry}^{eff} = \varepsilon^{\tau_l} k^{l} + k_{hp} \tag{10}$$

In addition, the contact resistance between the sample and plate and among fibers enters both measurements. Because the two measurements were conducted without disassembling the device, the contacting conditions are identical such as the compartment pressure and temperature, and hence the contact resistance is the same. Because the contact resistance is assumed to be spread uniformly throughout the medium, the subtraction on the left side of Eq. (10) cancels the contact resistance. Further, in the above equation the last term on the right is small at low temperature, and changes rapidly with temperature, while the first term on the right remains almost constant, as shown in Fig. 5. Thus, the heat pipe effect can be separated out by comparing the measurements at high and low temperatures.

4. Results and discussion

Fig. 8 presents the measured thermal conductivities of the hydrophilic carbon paper (0 wt.% PTFE loading) at different temperatures and liquid water saturations. The data show that the measured thermal conductivity for the dry case decreases with temperature: at 35 and 80 °C the measurements are about 0.6 and 0.4 W/m °C, respectively, smaller than that under well compression [3]. This value is between the measurements at low and high deformations [5], and along the line with Burheim et al. [7]. As to the decreasing trend, one reason is that the contact resistance between the fibers and the plate and among fibers is included in the measured data. It is difficult to eliminate it because of its dependence on compression pressure and the use of gasket. As temperature increases, the contact resistance may change as a result of the non-uniform thermal expansion of other components

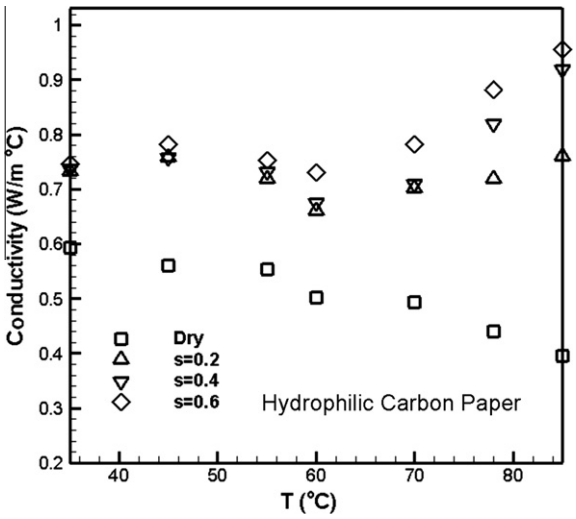

Fig. 8. The measured thermal conductivity of the hydrophilic carbon paper sample (0 wt.% PTFE loading).

such as the binding screws and gasket: in this case a decreasing trend is indicated. The changing contact resistance, however, has no effect on the measurement of the heat pipe effect and the liquid water contribution because the contact resistance is cancelled as explained in the preceding section. The measurement of the wet carbon papers is also plotted, showing increased conductance when adding liquid water.

Fig. 9 shows the added heat conductance due to liquid water presence inside the hydrophilic paper, i.e. Eq. (10). The measurement shows increasing conductivity with temperature in most cases. At 35 °C, Fig. 5 shows a weak heat pipe effect (about 0.05 W/m °C for $s = 0.4$), contributing a portion of the added conductance. The liquid water is conductive, which is another reason for the observed increase. The contribution of bulk liquid can be evaluated using the first term on the right of Eq. (10), $\varepsilon^{\tau_l} k^l$. Assuming liquid water follows a morphology between the solid matrix and pore network, the bulk water conductivity of 0.6 W/m °C (see Fig. 5), a tortuosity of 2.0, a saturation of 0.4, and porosity of 0.76 will yield a conductance around 0.055 W/m °C. A smaller tortuosity, i.e. less than 2.0, will yield a larger contribution, which will better match with the experimental data. Note that the solid matrix tortuosity is much larger than 2.0. Despite that in reality liquid water attaches the hydrophilic matrix, liquid may not follow the matrix morphology completely. Instead, it exists preferentially at fiber joints, reducing local thermal resistance, see Fig. 2(b). The solid matrix is made of fibers, which are placed randomly in the lateral direction and touch each other at their contacting points. Our previous study [10] directly simulated pore-level heat transfer, indicating that the through-plane heat conduction occurs via a route combining the lateral path along fibers and through-plane one at the contacting points, see Fig. 2(a). The cylindrical shape of fibers results in a small contacting area and hence large resistance. Consequently, the solid matrix's tortuosity was found to be over 10. Liquid presence at the contacting area, however, considerably improves local heat transfer by reducing the contact resistance among fibers, see Fig. 2(b).

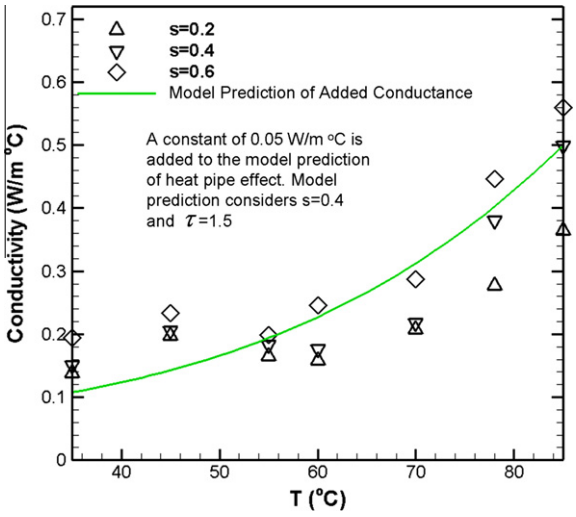

Fig. 9. The added thermal conductivity due to liquid water presence and model prediction for in the hydrophilic carbon paper.

In addition, the experimental data show the overall heat conductance increases with temperature in most cases, indicative of enhanced the heat pipe effect. A model prediction is also plotted for the liquid saturation of 0.4, showing a similar trend of thermal conductivity change. The model prediction assumes the vapor diffusion is the rate limiting step for the heat pipe effect. The liquid flow rate can be another limiting factor which explains the observed discrepancy between the experimental data and model prediction. This is particularly true for the fiber–matrix system, in which liquid inclines to attach the joint areas between fibers due to the hydrophilic nature of the surface, see Fig. 2(b). At a higher level of saturation, more liquid can be sent back to the evaporation surface, improving the heat pipe effect. Another possible reason for the observed conductance increase is the temperature-dependence of the bulk water conductivity: Fig. 5 shows that about 0.06 W/m °C will be added to water conductivity when temperature changes from 35 to 85 °C, which accounts for a minute portion of the increased thermal conductivity.

The wetting property of carbon paper is an important factor governing two-phase flow, see Fig. 2(b), (c), (e), and (f). Thus, a hydrophobic carbon paper likely exhibits a different heat-pipe effect. Fig. 10 displays the experimental data of a hydrophobic carbon paper with 30 wt.% PTFE loading. In this case, a slightly higher compression ratio 18 ± 3% was applied. This, along with the PTFE addition, may result in less change of thermal conductivity with temperature, as seen from the data of the dry sample. When liquid water is added, the overall thermal conductivity is slightly increased. For this medium, two liquid saturations, 0.2 and 0.4, were considered in the experiment because a larger uncertainty may arise when injecting high-content water in the nonwetting medium. However, the conductance increase with temperature is small.

Fig. 11 plots the added thermal conductivity due to liquid water presence. At 45 °C where heat pipe effect is relatively weak, the added conductance appears small in comparison with the hydrophilic one, with about 0.08 versus 0.16 W/m °C. One possible reason is due to the distinct morphologies of liquid presence in the two media: liquid tends to form isolated bulk droplets at a hydrophobic surface whereas it tends to form a film at the hydrophilic surface, see Fig. 2(e) and (f). Isolated droplets contribute smaller conductance; however, the droplet morphology makes it easier to link neighboring fibers, reducing tortuosity, see in Fig. 2(c). The final effect is determined by the balance of the two factors. Another possible reason is heat pipe effect, which is likely active only in a portion of the hydrophobic paper, to be detailed later. From 45 to 85 °C, the thermal conductivity is slightly increased by about 0.05 W/m °C, which again is much lower than that of the hydrophilic paper. This value is close to the increment of bulk water conductivity in the range of temperature increase, see Fig. 5. We also plot in the figure the liquid water conductivity from 45 to 85 °C with a liquid saturation of 0.3 (the average of the two experimental

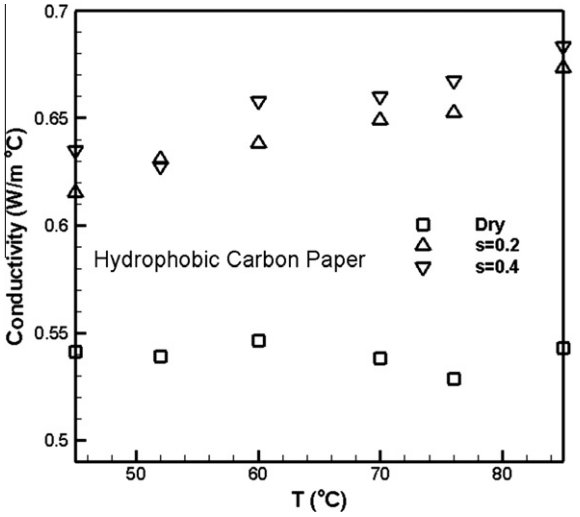

Fig. 10. The measured thermal conductivity of the hydrophobic carbon paper sample (30 wt.% PTFE loading).

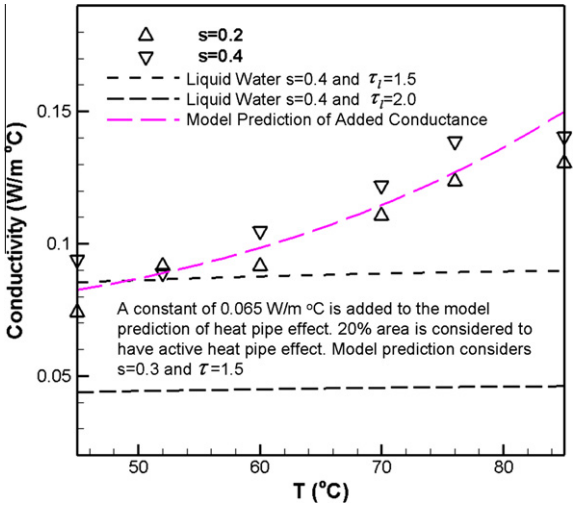

Fig. 11. The added thermal conductivity due to liquid water presence, and model prediction, and liquid water conductivity at $s = 0.4$ for the hydrophobic carbon paper.

saturations) using the Bruggeman correlation. Bulk liquid with the tortuosity of 1.5 contributes about 0.08 W/m °C to the conductivity at a temperature point. A higher tortuosity 2.0 gives a lower value, around 0.05 W/m °C. For both tortuosities, the temperature dependence of liquid thermal conductivity is negligible, less than 0.01 W/m °C increase is indicated when temperature changes from 45 to 85 °C. In addition, the heat pipe conductance predicted by Eq. (5) is much larger than the observation: the equation gives an increase of about 0.4 W/m °C in the apparent conductivity from 45 to 85 °C. A much small increase observed in the hydrophobic medium is possibly due to the lack of liquid flow back to the evaporator side: several experiment reported that a breakthrough pressure [15–18] is required to enable liquid water flow through hydrophobic carbon papers. Fig. 12 visualized droplet formation at the surface of a hydrophobic carbon paper, resulting from the water transport through the medium, and showed droplets always form at the two preferred locations. The routes to these sites exhibit small flow resistance, therefore are preferred for liquid flow. Similarly, the heat pipe effect is likely promoted in the portion of the medium where flow resistance is low and the

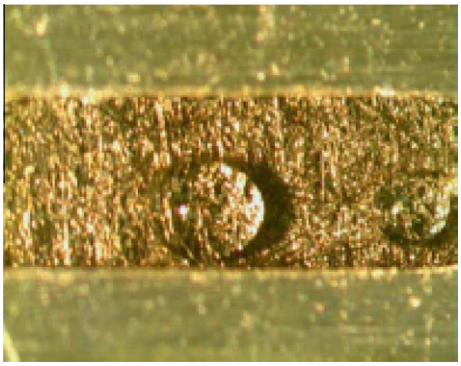

Fig. 12. Two preferred sites of liquid water droplet formation at the surface of a hydrophobic carbon paper [18]. The liquid droplets result from liquid water transport through the medium.

capillary pressure is sufficiently large to overcome the breakthrough pressure, see the dashed line in Fig. 2(f). As a result, heat pipes are active only in these local spots, resulting in a significantly reduced effect, as observed. We assume the heat pipe effect is active in a 20% portion of the carbon paper, and obtain a similar trend of thermal conductance increase as the experimental data.

5. Conclusion

This paper presented an experimental study of the thermal conductivity of carbon papers with/out liquid presence and the heat pipe effect. An experimental setup was designed and measurement was carried out for both hydrophilic and hydrophobic carbon papers. We found that the overall conductivity is improved when liquid water is added to the carbon papers, and the overall conductivity in wet media increases with temperature. By separating out the thermal conductivity of dry carbon papers, the added conductivity due to liquid water presence was obtained. For the hydrophilic paper, the measured data showed an increase of conductivity at 35 °C, which is larger than that of the predicted heat pipe effect. It is possibly due to the fact that liquid is presented preferentially at the contact area among fibers, which greatly reduces the local resistance. For the hydrophobic carbon paper, the increase is smaller than the hydrophilic because of difference in either liquid morphology or heat pipe effect. Under high temperature, heat pipe effect becomes significant, improving the overall thermal conductivity of the hydrophilic papers. The added conductance increases rapidly with temperature with about 0.4 W/m °C from 35 to 85 °C. The model prediction showed a similar trend as the experimental data. The heat pipe effect is smaller for the hydrophobic carbon paper, which is likely due to its nonwetting surface: liquid water only flows back to the evaporation surface via preferred routes at the breakthrough pressure. As a result, the heat pipe effect is active in part of the hydrophobic media, yielding a reduced increase in added thermal conductivity with temperature.

References

[1] M. Mathias, J. Roth, J. Fleming, W. Lehnert, Diffusion media materials and characterization, in: W. Vielstich, H. Gasteiger, A. Lamm (Eds.), Handbook of Fuel Cells: Fundamentals, Technology and Applications, vol. 3, John Wiley & Sons, Ltd., 2003.
[2] Y. Wang, K.S. Chen, J. Mishler, S.C. Cho, X.C. Adroher, A review of polymer electrolyte membrane fuel cells: technology, applications, and needs on fundamental research, Appl. Energy 88 (2011) 981–1007.
[3] E.S. Platunov, Instruments for measuring thermal conductivity, thermal diffusivity, and specific heat under monotonic heating, in: K.D. Maglic, A. Cezairliyan, V.E. Peletsky (Eds.), Compendum of Thermophysical Property Measurement Methods: Recommended Measurement Techniques and Practices, vol. 2, Plenum Press, 1989, pp. 347–374.

[4] M. Khandelwal, M.M. Mench, Direct Measurement of Through-Plane Thermal Conductivity and Contact Resistance in Fuel Cell Materials, J. Power Sources 161 (2006) 1106.
[5] N. Zamel, E. Litovsky, X. Li, J. Kleiman, Measurement of the through-plane thermal conductivity of carbon paper diffusion media for the temperature range from −50 to +120 °C, Int. J. Hydrogen Energy 36 (2011) 12618–12625.
[6] O. Burheim, P.J.S. Vie, J.G. Pharoah, S. Kjelstrup, Ex situ measurements of through-plane thermal conductivities in a polymer electrolyte fuel cell, J. Power Sources 195 (2010) 249–256.
[7] O. Burheim, J.G. Pharoah, H. Lampert, Through-plane thermal conductivity of PEMFC porous transport layers, J. Fuel Cell Sci. Technol. 8 (2011) 021013–021021.
[8] Y. Wang, C.Y. Wang, A non-isothermal, two-phase model for polymer electrolyte fuel cells, J. Electrochem. Soc. 153 (2006) A1193–A1200.
[9] Y. Wang, C.Y. Wang, Two-phase transients of polymer electrolyte fuel cells, J. Electrochem. Soc. 154 (2007) B636–B643.
[10] Y. Wang, S. Cho, R. Thiedmann, V. Schmidt, W. Lehnert, X. Feng, Stochastic modeling and direct simulation of the diffusion media for polymer electrolyte fuel cells, Int. J. Heat Mass Transfer 53 (2010) 1128–1138.
[11] R.J. Moffat, Describing the Uncertainties in Experimental Results, Exp. Therm. Fluid Sci. 1 (1988) 3.
[12] E.C. Kumbur, K.V. Sharp, M.M. Mench, A Validated Leverett Approach to Multiphase Flow in Polymer Electrolyte Fuel Cell Diffusion Media: Part 1: Hydrophobicity Effect, Journal of the Electrochemical Society 154 (2007) B1295–B1304.
[13] J.T. Gostick, M.W. Fowler, M.A. Ioannidis, M.D. Pritzker, Y.M. Volfkovich, A. Sakars, Capillary pressure and hydrophilic porosity in gas diffusion layers for polymer electrolyte fuel cells, J. Power Sources 156 (2006) 375.
[14] S. Escribano, J.-F. Blachot, J. Eth'eve, A. Morin, R. Mosdale, Characterization of PEMFCs gas diffusion layers properties, J. Power Sources 156 (2006) 8–13.
[15] S. Litster, D. Sinton, N. Djilali, Ex situ Visualization of Liquid Water Transport in PEM Fuel Cell Gas Diffusion Layers, J. Power Sources 154 (1) (2006) 95–105.
[16] B. Gao, T.S. Steenhuis, Y. Zevi, J.Y. Parlange, R.N. Carter, T.A. Trabold, Visualization of Unstable Water Flow in a Fuel Cell Gas Diffusion Layer, J. Power Sources 190 (2) (2009) 493–498.
[17] T.-L. Liu, C. Pan, Visualization and back pressure analysis of water transport through gas diffusion layers of proton exchange membrane fuel cell, J. Power Sources 207 (2012) 60–69.
[18] Y. Wang, Porous-media flow fields for polymer electrolyte fuel cells II. Analysis of channel two-phase flow, J. Electrochem. Soc. 156 (2009) B1134–B1141.
[19] S.C. Cho, Y. Wang, Private communication, 2012.